Controllable oxidation and degradation of lignin via H_2O_2–O_3：From biomass into retanning agent for sustainable leather manufacturing

Ningqiang You[1,2], Yue Yu[1,2,3*], Ya-nan Wang[1,2,3], Bi Shi[1,2,3]

1 National Engineering Laboratory for Clean Technology of Leather Manufacture, Sichuan University, No. 24 South Section 1, Yihuan Road, Chengdu 610065, China

2 Key Laboratory of Leather Chemistry and Engineering, (Sichuan University), Ministry of Education, Chengdu 610065, China

3 College of Biomass Science and Engineering, Sichuan University, No. 24 South Section 1, Yihuan Road, Chengdu 610065, China

*Corresponding Author, E-mail: yuyue@scu.edu.cn.

Abstract

Biomass-derived retanning agents are considered promising substitutes for aromatic syntans (AS). Here, a synergistic H_2O_2–O_3 oxidation system was developed to oxidize lignin (LG) for the preparation of oxidized lignin (OLG). FT-IR, ^{13}C NMR, and 2D HSQC NMR characterization confirmed that the oxidation process cleaved aliphatic side-chain linkages (β-O-4, β-5, and β-β'), induced aromatic ring-opening reactions, and transformed phenolic hydroxyl and methoxy groups into carboxyl groups, thereby reducing chromaticity. Free radical quenching experiments and EPR analysis revealed that the H_2O_2–O_3 system obviously enhanced hydroxyl radical generation. ESI-MS analysis of the oxidation products of model compound (2-methoxy-4-propylphenol) revealed that H_2O_2–O_3, H_2O_2, and O_3 oxidation systems produced aliphatic carboxylic acids as final products, while the H_2O_2–O_3 system exhibited a greater number of intermediates and more diversified reaction pathways, leading to superior oxidative efficiency. OLG, featuring an optimized carboxyl content (8.2 mmol/g), phenolic hydroxyl content (0.17 mmol/g), and a molecular weight of 735, demonstrated excellent penetration ability into the leather matrix. This facilitated coordination with Cr(III), thereby forming a robust multi-point crosslinked network between collagen fibers. Thus, the OLG retanning agent achieved a Ts of 115.4°C, a 25.3% increase in thickness, and remarkable softness and mechanical strength. Life cycle assessment

revealed that, compared with the AS retanning system, the OLG retanning system achieved a 61.7% reduction in carbon emissions and a 71.6% decrease in resource consumption, highlighting its potential as an eco-friendly alternative. This study offers new insights into low-carbon retanning systems and presents a feasible strategy for the valorization of LG.

1. Introduction

Retanning, often considered a critical step in leather processing, minimizes variations in leather properties across different sections of the hide, thereby increasing yield and imparting desirable fullness and elasticity (Ning et al., 2022). Commonly used retanning agents include aromatic syntans, amino resins, acrylic resins, and aldehyde derivatives. Among these, aromatic syntans, especially phenolic syntans, are favored for their superior filling properties and dispersibility (Sun et al., 2021). However, European Union regulations restrict bisphenol A levels in leather and limit the use of bisphenol A-containing chemicals in leather production. Furthermore, aromatic syntan production requires significant petrochemical inputs (e.g., propylene and benzene) and contributes to greenhouse gas emissions (Liu et al., 2022). Additionally, aromatic syntans may release formaldehyde during post-tanning treatments (Thanikaivelan et al., 2007). Consequently, research and development efforts are increasingly focused on biomass-derived retanning agents to replace aromatic syntans, reduce formaldehyde release, and lower carbon emissions, reflecting a key trend in the leather industry.

Biomass is primarily composed of cellulose, hemicellulose, and lignin (Jiang et al., 2021). While cellulose and hemicellulose are widely utilized in the pulp and paper industry, the associated processes generate black liquor, a lignin-rich byproduct. Despite the annual extraction of approximately 50 million tons of lignin from biomass, only a small fraction (2%) is valorized, predominantly into low-value products like dispersants and adhesives (Sen et al., 2015). Consequently, the conversion of lignin into high-value chemicals is crucial for enhancing biomass utilization. Lignin is a complex, three-dimensional aromatic biopolymer composed of guaiacyl, syringyl, and *p*-hydroxyphenyl units linked by various bonds, including β-O-4, β-5, and β-β', and further characterized by hydroxyl and carbonyl groups on its aliphatic side chains (Espinoza-Acosta et al., 2018). Due to its structural similarity to aromatic syntans, chemically

modified lignin exhibits potential as a retanning agent. However, research on lignin-based retanning agents remains scarce. For example, Balasubramanian et al. (2017) and Zakir et al. (2015) extracted soluble lignin from black liquor through pH adjustment, while Vedhanayagam et al. (2015) employed sulfonation and formaldehyde condensation to modify lignin. A significant challenge in these methods is the generation of dark-colored products, which considerably restricts the industrial applicability of lignin.

Oxidation is an economically viable and operationally simple method for lightening the color the lignin, making it practical for industrial applications. Lawoko et al. (2024) investigated the effects of H_2O_2 oxidative reactions under acidic conditions on lignin's molecular structure, showing that phenolic ring-opening leads to carboxylic acid formation and side-chain oxidation. Figueiredo et al. (2020) found that O_3 oxidation decomposed 52%-87% of industrial lignin, forming dibasic acids and esters in bio-oil (Wang et al., 2020). However, both H_2O_2 and O_3 oxidation have limited efficiency, hindering the development and application of oxidized lignin. The H_2O_2–O_3 process, commonly used for colored wastewater treatment (Yadav et al., 2022), produces two ·OH radicals from two O_3 molecules and one H_2O_2 molecule, with a redox potential of 2.8 eV (Takeuchi et al., 2017). This method is efficient and multifunctional, accelerating degradation rates and reducing toxic by-products (Chen et al., 2024). For lignin, H_2O_2–O_3 may have the potential of oxidizing hydroxyl and methoxyl groups into carboxyl groups (Figure 1), which can coordinate with Cr(III) and form electrovalent bonds with protonated amino groups. Thus, oxidized lignin may form a robust multi-point crosslinking network among collagen fiber, thereby strengthening the retanning performance.

Figure 1. Proposed mechanism of lignin oxidation and its applications.

This study established a H_2O_2–O_3 synergistic oxidation system, as well as separate H_2O_2 and O_3 systems as controls. The main objective was to produce light-colored oxidized lignins (OLGs) with appropriate functional group content and molecular weight. The chemical characterization of the OLGs included size exclusion chromatography (SEC), Fourier transform infrared spectroscopy (FT–IR), and nuclear magnetic resonance (NMR). Electron paramagnetic resonance (EPR) and radical quenching experiments were performed to identify the active species generated during oxidation. To clarify the oxidation mechanism, a model compound (2-methoxy-4-propylphenol) was oxidized and analyzed using electrospray ionization mass spectrometry (ESI–MS). Finally, the OLGs were utilized in leather retanning, followed by an evaluation of the properties of the retanned leather and a life cycle assessment (LCA) to analyze the environmental benefits.

2. Materials and methods

2.1. Materials

Lignin was procured from Shandong Longli Biotechnology Co., Ltd. H_2O_2 (30 wt%) was purchased from Chengdu Kelong Chemical Co., Ltd. Amberlite IR120 H^+-form strong-acid cation exchange resin was obtained from Shanghai Sigma-Aldrich Co., Ltd. Wet blue leather was supplied by Shandong Senlu Leather Industry Co., Ltd. Industrial-grade chemicals were utilized for leather processing, whereas analytical-grade reagents were employed for all analyses.

2.2. Preparation of OLGs

The experimental setup is schematically illustrated in Figure 2. Lignin (30 g) was dissolved in 210 g of deionized water within a 1 L reactor. Subsequently, NaOH (1.5 g) was added to adjust the pH to approximately 10.0. The mixture was heated to 70°C under continuous stirring at 500 rpm for 10 min to ensure complete dissolution of lignin. A constant flow pump was employed to introduce H_2O_2 into the reactor at a controlled flow rate of 12 g/h. Simultaneously, O_3, generated by an oxygen-fed ozone generator (WH-H-Y10A, Wohuan Technology Co., Ltd., China) operating at 0.45 A and producing 7.5 g/h, was continuously fed into the reactor. Throughout the reaction process, a NaOH solution (1.75 mol/L) was introduced into the reactor to maintain the pH within the range of 8.0–9.0. This combined treatment involving both H_2O_2 and O_3 was designated

as the H_2O_2–O_3 group. For comparison, experiments were also conducted using either H_2O_2 or O_3 alone at the same feeding rates; these were designated as the H_2O_2 and O_3 groups, respectively. The group without any oxidation operation served as the control. The reaction proceeded under vigorous stirring for 5 hours to produce OLGs. During the reaction, samples were collected for colority and structural characterization. The tail gas produced during the reaction was directed into a saturated Na_2SO_3 solution for safe disposal.

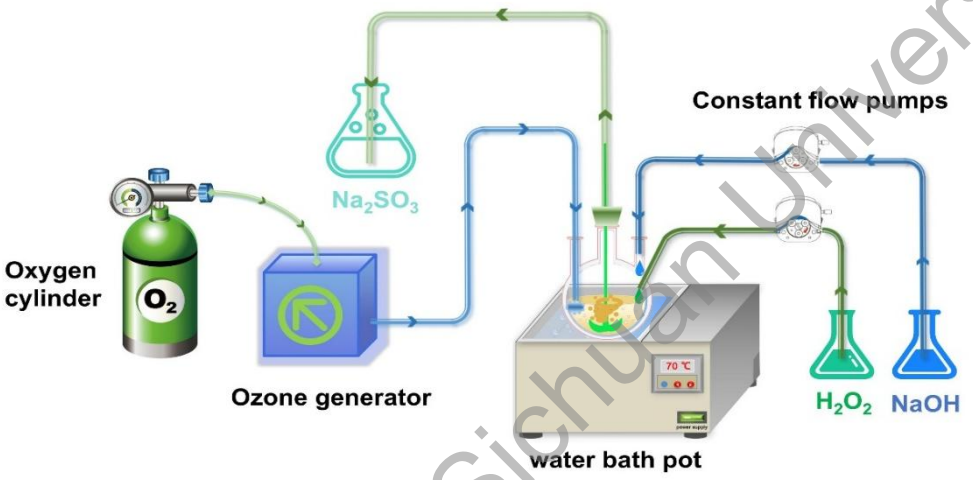

Figure 2. Illustration of the experimental setup.

2.3. Colority and structure characterization

The colority of LG and OLGs was determined using the platinum-cobalt colorimetric method (Wang et al., 2022a). The weight-average molecular weight (M_w), number-average molecular weight (M_n), and polydispersity index (M_w/M_n) of LG and OLGs (10 g/L) were analyzed by SEC using an Agilent 1260 Infinity II system equipped with a TSK GPC GMPWXL column (7.8 mm × 300 mm, Tosoh, Japan) and a refractive index detector. The mobile phase consisted of 0.1 mol/L Na_2HPO_4 and acetonitrile (8:2, *v/v*) at a flow rate of 0.6 mL/min. The phenolic hydroxyl content of LG and OLGs was determined using the Folin-Ciocalteu reagent method (Zhang et al., 2020). The carboxyl content of OLGs was measured by acid-base titration (Yu et al., 2017). LG and OLGs were lyophilized using a Christ Beta 1–8 LD plus freeze dryer (Christ, Germany). Color parameters (L, a, b) of the lyophilized samples were measured using a colorimeter (CR-13, Konica

Minolta, Japan), and the color difference (ΔE) between the lyophilized samples and a standard white reference (L = 93.8, a = 0.5, b = 3.6) was calculated (Belasco et al., 2020). FT-IR spectra of the lyophilized samples were acquired using a Thermo Scientific Nicolet 6700 spectrometer (Thermo Scientific, USA) at a resolution of 2 cm^{-1}. ^{13}C and two-dimensional heteronuclear single quantum correlation (2D-HSQC) NMR spectra of the lyophilized LG and OLGs were recorded on a Bruker Avance NEO 600 NMR spectrometer (Bruker, Germany). For ^{13}C NMR, 400 mg samples were dissolved in 1 mL D_2O. For 2D-HSQC NMR, 100 mg samples were dissolved in 1 mL DMSO-d_6. The surface morphologies of the lyophilized samples were observed using scanning electron microscopy (SEM, JEOL JSM-7500 F, JEOL, Japan).

2.4. Detection and quenching of free radicals

The OLGs were synthesized according to the experimental protocol outlined in Section 2.2, with an oxidation time of 5 h. Glycerol, serving as a free radical quenching agent, was continuously fed into the reactor at a rate of 7.5 g/h (Hwang et al., 2010) during the oxidation process. Carboxyl content analysis was then performed on the resulting products, both with and without the inclusion of glycerol as a quenching agent.

The generation of hydroxyl radicals was assessed using EPR spectroscopy. A reactor was charged with 1 mmol DMPO (5,5-dimethyl-1-pyrroline N-oxide, spin-trapping agent), 9 mL of deionized water, and 1 g of lignin. The mixture was oxidized for 4 min via continuous feeding of either H_2O_2 (0.2 g/min), O_3 (0.125 g/min), or a combination of H_2O_2 (0.2 g/min) and O_3 (0.125 g/min). Following oxidation, the reaction was allowed to proceed for an additional 4 min, and samples were then collected for EPR analysis using a Bruker EMXplus X-band spectrometer (Zhou et al., 2020). A control group without lignin was included for comparison.

2.5. Preparation and analysis of oxidized lignin model

2-methoxy-4-propylphenol, a lignin model compound, was oxidized using H_2O_2–O_3, H_2O_2, and O_3 systems as detailed in Section 2.2. Following oxidation, the reaction products were diluted with methanol to a concentration of 5×10^{-3} mg/mL, filtered through a 0.45 μm organic solvent-resistant membrane, and analyzed by ESI–MS (ESI-LCMS-IT-TOF, Shimadzu, Japan). Direct infusion mass spectrometry was conducted with the following parameters: injection volume

of 1.0 μL, spray voltage of 4.5 kV, detector voltage of 1.60 kV, electrospray interface temperature of 250 °C, and a mass-to-charge (m/z) range of 50–300 (Arulselvan et al., 2023).

2.6. Retanning trials

Wet blue leather samples (60 cm × 50 cm, 1.2 mm thickness) were rewetted, neutralized, and subsequently retanned with 10 wt% OLGs (based on the weight of wet blue leather) with varying degrees of oxidation. A control group without OLGs and a comparison group retanned with aromatic syntan (AS) were included for comparative analysis. Following retanning, fatliquoring was performed. The detailed post-tanning process is outlined in Table 1. The shrinkage temperature (Ts) of the crust leather was measured using an MSW-YD4 shrinkage temperature tester (Sunshine Electronic Research Institute, China). The thickness increase rates of different groups were determined using a MY-3130-A2 digital desktop thickness gauge (Mingyu Electronic Technology Co., Ltd., China). Additionally, the softness, compression properties, resilience, tear strength, bursting strength, tensile strength, and elongation at break of the crust leathers were evaluated as described by Yu et al. (2020). A life cycle assessment (LCA) was conducted to evaluate the impacts on resource consumption, climate change, ecosystem quality, and human health. The system boundary for the LCA extended from the rewetting stage through the fatliquoring stage. The WebLCA open platform (eFootprint, IKE Environmental Technology Co. Ltd., China) was utilized to model the retanning systems and calculate impact categories, including global warming potential (GWP), primary energy demand (PED), abiotic depletion potential (ADP), acidification potential (AP), eutrophication potential (EP), water use (WU), human toxicity cancer effects (HTC), human toxicity non-cancer effects (HTNC), and ecotoxicity freshwater (ET).

Table 1 Post-tanning process

Process	Chemicals	Temperature (°C)	Content (%)	Time (min)	Remarks
Rewetting	Water	35	400		
	Degreasing agent		0.5		

	HCOOH		0.3	40	Drain
	Water	35	200		
Neutralization	HCOONa		1	30	
	$NaHCO_3$		0.6×n	15×n+60	pH 6.0
	Water	35	400	10	Drain
	Water	35	100		
Retanning	Control/AS/OLGs		10	60	
	HCOOH		0.5×2	10+30	pH 4.0, Drain
	Water	50	150		
Fatliquoring	Fatliquors		20	60	
	HCOOH		0.4×2	15×2	pH 3.8, Drain
Washing	Water	25	200	15	Drain
Horse up overnight →Hang drying → Conditioning → Milling → Crust leathers					

3. Results and discussion

3.1. Colority of OLGs

The oxidative treatment was designed to introduce carboxyl groups into the lignin molecular structure while disrupting its chromophoric structures to achieve decolorization (Xue et al., 2023). We systematically evaluated the decolorization efficiency of three oxidation systems (H_2O_2, O_3, and H_2O_2–O_3) on lignin. As shown in Fig. 3a, the chromaticity of OLGs stabilized after 5 h across all systems, with the H_2O_2–O_3 group achieving the lowest equilibrium chromaticity, followed by O_3 and H_2O_2. Notably, the H_2O_2–O_3 system exhibited the fastest decolorization rates during the initial 5 h, surpassing both H_2O_2 and O_3. The O_3 system exhibited a delayed oxidation capability, with a significantly accelerated decolorization process observed after 3 h of oxidation. Remarkably, after 10 h of oxidation, the oxidant dosage required for both the H_2O_2 and O_3 systems was equivalent to that of the H_2O_2–O_3 system within 5 h. However, the colority of the H_2O_2–O_3 oxidation product was obviously lower than that of the H_2O_2 and O_3 systems, indicating the presence of a synergistic decolorization effect in the H_2O_2–O_3 system. Visual comparisons of liquid and solid samples after 5 h of oxidation (Fig. 3b) revealed that OLG treated with the H_2O_2–

O_3 system exhibited the lightest coloration, appearing nearly white. Quantitative analysis of chromaticity reduction (Figs. 3c–d) further demonstrated the superior performance of the H_2O_2–O_3 system, achieving a total color difference reduction of 43.5, which significantly exceeded the cumulative additive effect of individual H_2O_2 (10.3) and O_3 (10.4) treatments (20.7 in total). These findings confirm that the H_2O_2–O_3 synergistic oxidation system achieves optimal decolorization efficiency.

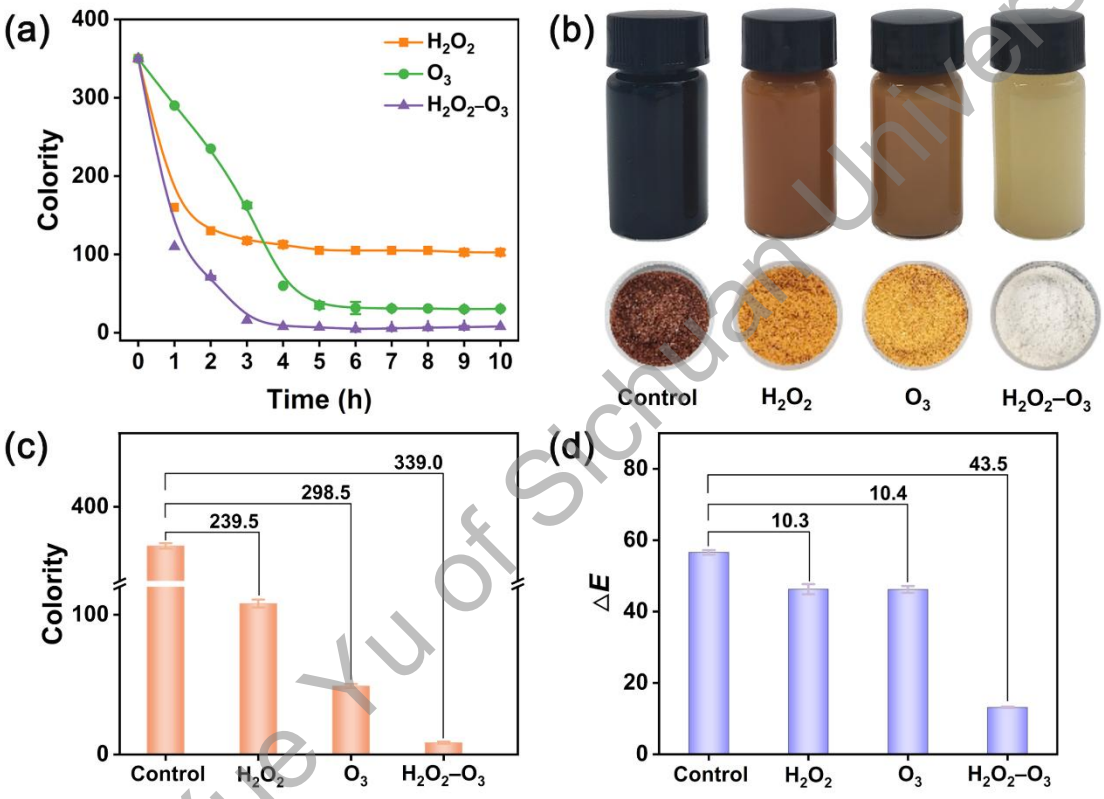

Fig. 3. Color changes of OSLs during oxidation (a); Appearance of liquid and solid OSL products (b); Color of liquid products (c) and △E of solid products (d) after 5h oxidation with different oxidants.

3.2. Chemical structure of OLGs.

The molecular size of tanning agents plays a critical role in determining their penetration ability in leather (Guo et al., 2021; Yu et al., 2020). By analyzing the molecular weight (*M*w) and *M*w distribution of LG and OLGs (Fig. 4a), it is evident that the *M*w of LG is much higher than

that of OLGs, suggesting that all three oxidation systems induce the degradation of LG. Notably, the *M*w of LG is obviously reduced after treatment with O_3 and H_2O_2–O_3, whereas the degradation caused by H_2O_2 alone is relatively less pronounced. The analysis of functional group content in OLGs reveals that the phenolic hydroxyl group (Ph-OH) content in the H_2O_2–O_3 sample is the lowest, at 0.17 mmol/g (Fig. 4b), while the carboxyl group content is the highest, reaching 8.2 mmol/g (Fig. 4c). The obvious increase in carboxyl group content far exceeds the reduction in Ph-OH content, indicating that H_2O_2–O_3 not only oxidizes Ph-OH but also induces benzene ring cleavage, leading to the formation of additional carboxyl groups (Fernandesa et al., 2019). This conclusion is further supported by FT-IR analysis (Fig. 4d), where the absorption peak intensity at 1650 cm^{-1}, corresponding to the carbonyl group (Shen, H.C et al., 2022), shows a marked increase after oxidation, particularly for the H_2O_2–O_3 sample. Additionally, ^{13}C NMR analysis revealed that oxidation disrupts the G-unit structure of lignin and decreases the methoxy group content while increasing the carboxyl group content (Fig. 4e). Notably, the H_2O_2–O_3 sample exhibits the highest carboxyl group content, accompanied by the weakest signals for the G-unit and methoxy groups (Hilde et al., 2022). In contrast, the H_2O_2 sample shows a methoxy group content in the G-unit comparable to that of LG, suggesting that the ring-opening reaction is less extensive and the degree of oxidation is relatively milder in this sample. SEM images of LG and OLGs show that LG particles exhibit varying sizes with smooth and flat surfaces. Upon H_2O_2 treatment, a slight change in particle size occurs, and surface wrinkles begin to appear. Following O_3 oxidation, numerous fine pores and a few pits develop on the surface, while the blocky structure remains relatively well-defined. In contrast, after H_2O_2–O_3 oxidation, the lignin surface displays pronounced wrinkling, featuring the largest number of large pores and a significant reduction in the size of blocky structures. These observations suggest that H_2O_2–O_3 treatment induces the highest degree of oxidation in lignin and results in superior porosity within its microstructure. In summary, the H_2O_2–O_3 sample shows the highest degree of oxidation, characterized by the lowest Ph-OH content and the highest carboxyl group content. This feature may enhance its coordination ability with Cr^{3+}. Additionally, its lowest molecular weight confers superior penetration ability in leather (Covington et al., 1997). Thus, the H_2O_2–O_3 sample appears to be the most suitable candidate for use as a retanning agent.

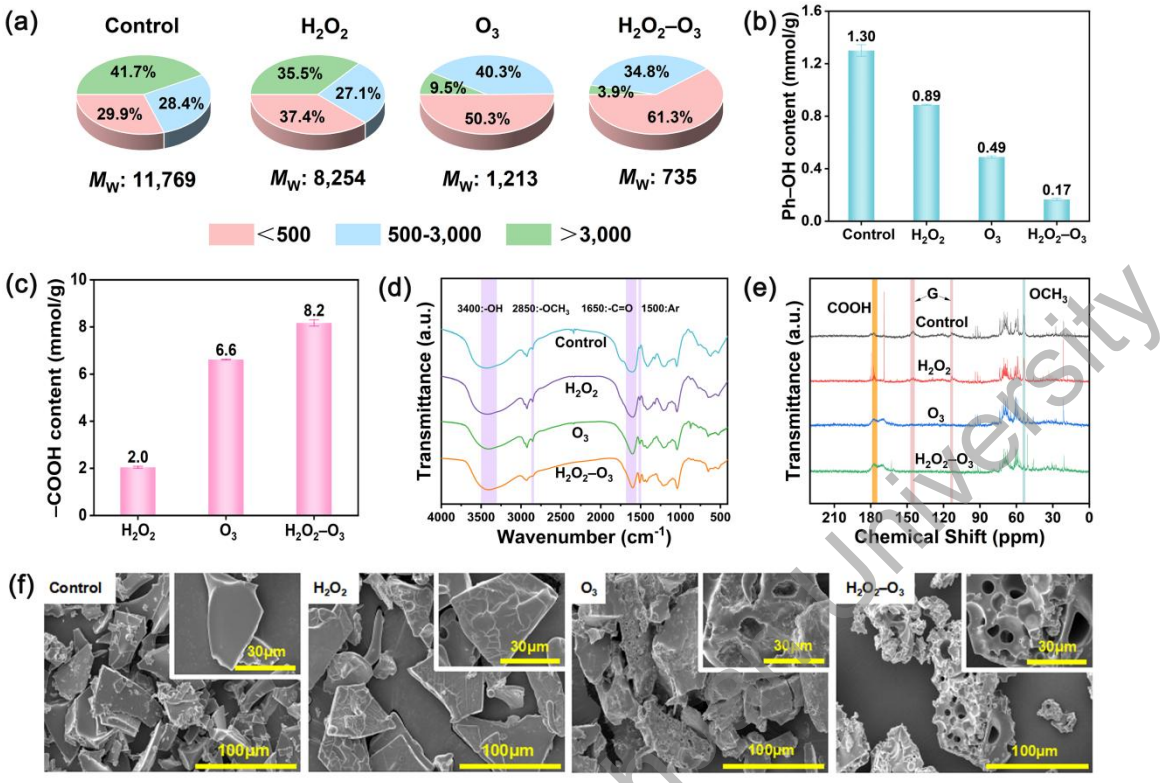

Fig. 4. M_w distribution (a); Ph-OH (b) and carboxyl (c) content of oxidant products; FT-IR spectra (d) and ^{13}C NMR (e) of LG and OLGs; SEM images of LG and OLGs (f).

2D-HSQC spectra further elucidate the oxidation reaction of LG. The 2D-HSQC spectrum (Fig. 5) is divided into the aliphatic side-chain C–H region (δ_C/δ_H 50–90/3.0–5.5 ppm) and the aromatic C–H region (δ_C/δ_H 100–150/6.0–8.0 ppm) (Dong et al., 2022), with the assignments of substructures detailed in Table 2 (Jiang et al., 2021). In the aliphatic side-chain C–H region, the main connection types between the aromatic monomers of LG are the A structure (*β*-arylether, *β*-O-4), followed by the B (phenylcoumaran, *β*-5') and C (*β*-*β*') connection structures. Additionally, a CL condensation structure exists, with its main C–H signal located at δ_C/δ_H 55.5/3.7 ppm, corresponding to the methoxy group. In the aromatic C–H region, the primary monomer structures are G (guaiacyl) and S (syringyl), along with a small amount of H (p–hydroxyphenyl). After oxidation, the signals of the A, B and C structures weaken, indicating cleavage of the aliphatic side chains and a decrease in *M*w. The attenuation of the G, S, and H signals suggests ring-opening of the phenolic rings (Areskogh et al., 2010). Among the treated samples, the lignin

substructure signals in the H_2O_2–O_3 system are the weakest, suggesting the highest degree of oxidation and carboxyl group content. In the O_3 sample, the weakening of the signals in the aliphatic side-chain region is relatively mild, whereas the aromatic structure undergoes severe damage. This phenomenon arises because O_3 exhibits strong affinity for the aromatic structural units of lignin and possesses a higher oxidizing ability toward phenolic structures (Kulwinder et al., 2010). By contrast, H_2O_2 demonstrates weaker oxidizing power, leading to less extensive oxidation of lignin substructures, a larger *M*w, and retention of more lignin-related structures, which results in a darker product color.

All above results indicate that the ring-opening and oxidation of benzene rings predominantly occur near Ph-OH and methoxy groups (Areskog et al., 2010; Yang et al., 2021). Among the treatments, H_2O_2–O_3 exhibits the strongest oxidizing ability toward lignin structures, resulting in the highest carboxyl group content. In comparison with the O_3 group, further oxidation of the aliphatic side chains in the H_2O_2–O_3 treatment causes a more significant reduction in *M*w.

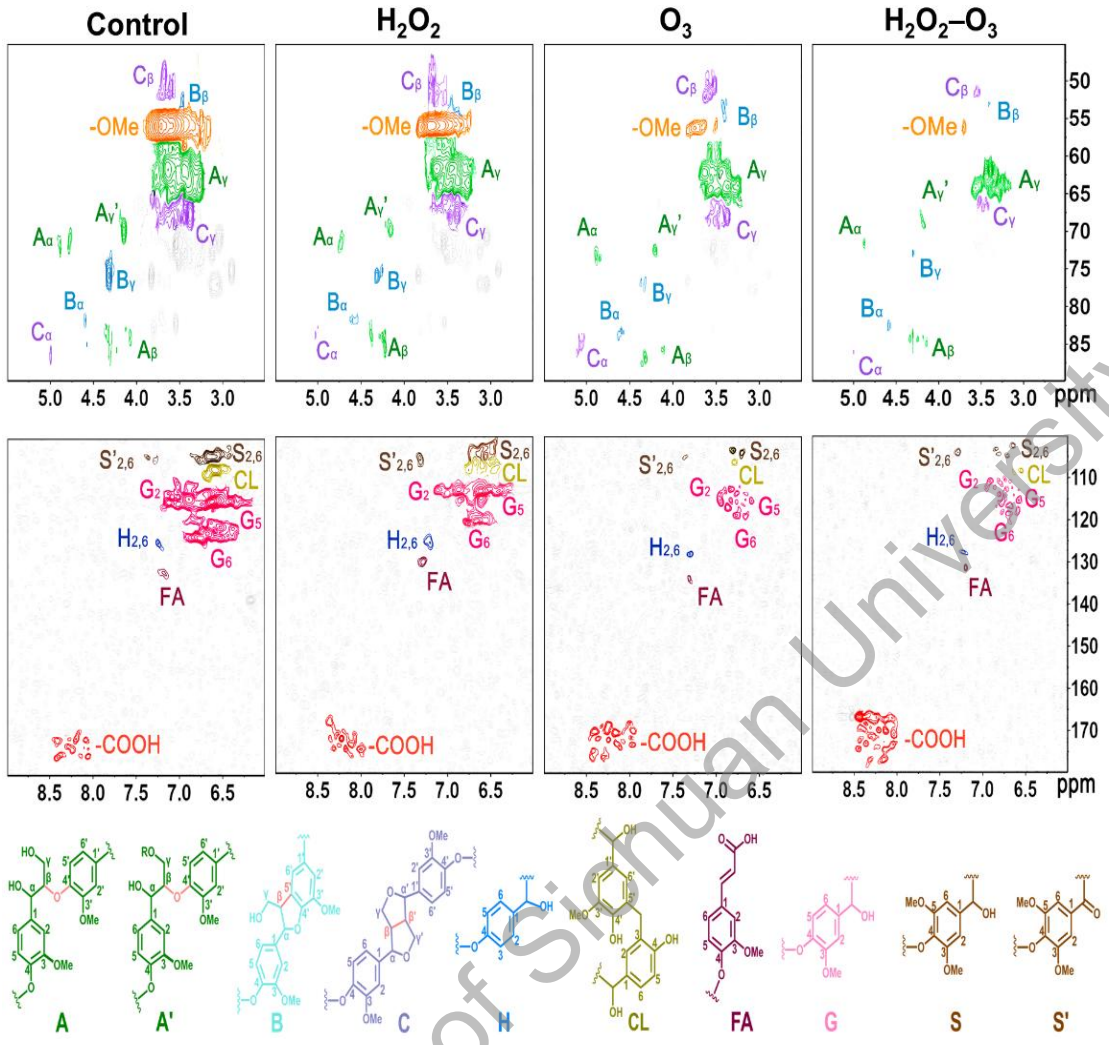

Fig. 5. 2D HSQC NMR spectra of LG and OLGs.

Table 2. Assignment of lignin units ^{13}C-^{1}H cross-signals in 2D HSQC-NMR spectra

Regions	Substructures	Labels	δ_C/δ_H (ppm)	Assignments
Aliphatic	OMe	C-H	55.5/3.71	C-H in methoxyls
side-chain	A	A_α	71.8/4.82	C_α-H_α in *β*-O-4′ linkages
		A_β	85.8–83.4/4.42–4.12	C_β-H_β in *β*-O-4′ linkages
		A_γ	59.5/3.75–3.35	C_γ-H_γ in *β*-O-4′ linkages
	A’	A_γ'	64.1/4.18	C_γ-H_γ in *β*-O-4′ linkages
	B	B_α	84.1/4.62	C_α-H_α in *β*-5′ linkages
		B_β	52.3/3.41	C_β-H_β in *β*-5′ linkages

Regions	Substructures	Labels	δ_C/δ_H (ppm)	Assignments
		B_γ	73.2/4.29	C_γ-H_γ in *β*-5′ linkages
	C	C_α	85.0/5.03	C_α-H_α in *β*-*β*′ linkages
		C_β	53.8/3.55	C_β-H_β in *β*-*β*′ linkages
		C_γ	66.4/3.52	C_γ-H_γ in *β*-*β*′ linkages
Aromatic	G	G_2	110.1/6.92	C_2-H_2 in guaiacyl units
		G_5	115.2/6.75	C_5-H_5 in guaiacyl units
		G_6	118.8/6.75	C_6-H_6 in guaiacyl units
	S	$S_{2,6}$	103.8/6.60–6.88	$C_{2,6}$-$H_{2,6}$ in syringyl units
	S’	$S_{2,6}'$	105.5/7.30	$C_{2,6}$-$H_{2,6}$ in oxidized syringyl units
	H	$H_{2,6}$	127.8/7.25	$C_{2,6}$-$H_{2,6}$ in p-hydroxyphenyl units
	COOH	C-H	172.0–178.0/8.0–8.4	C-H next to carboxyl groups

3.3. Role of hydroxyl radicals in oxidation

Radical-mediated mechanisms play a critical role in lignin oxidation (Ma et al., 2024). Here, the radical scavenger glycerol was employed to react with hydroxyl radicals (·OH), forming water and glyceroxyl radicals, thereby effectively suppressing ·OH activity (Fig. 6d) (Li et al., 2024). Upon introducing quenching agents into the H_2O_2–O_3 system, the carboxyl content in OLGs decreased from 8.2 to 3.1 mmol/g (Fig. 6a), confirming ·OH as the primary driver of carboxylation. EPR analysis (Figs. 6b-c) demonstrated obviously higher ·OH generation in the H_2O_2–O_3 system compared to H_2O_2 or O_3 alone. The O_3 system exhibited minimal ·OH due to its poor aqueous solubility and reliance on indirect oxidation pathways (Kulwinder et al., 2022). Lignin (LG) addition enhanced ·OH production in the H_2O_2 and H_2O_2–O_3 systems but induced superoxide radicals ($\cdot O_2^-$) in the O_3 system, indicating ozone-dominated direct oxidation with negligible ·OH contribution (Ge et al., 2022). The synergistic H_2O_2–O_3 system overcame the low efficiency of O_3 while generating stronger ·OH oxidants than H_2O_2 alone. This ·OH-driven mechanism accounts for its superior oxidative capacity and decolorization performance, making it particularly suitable for eco-friendly leather retanning.

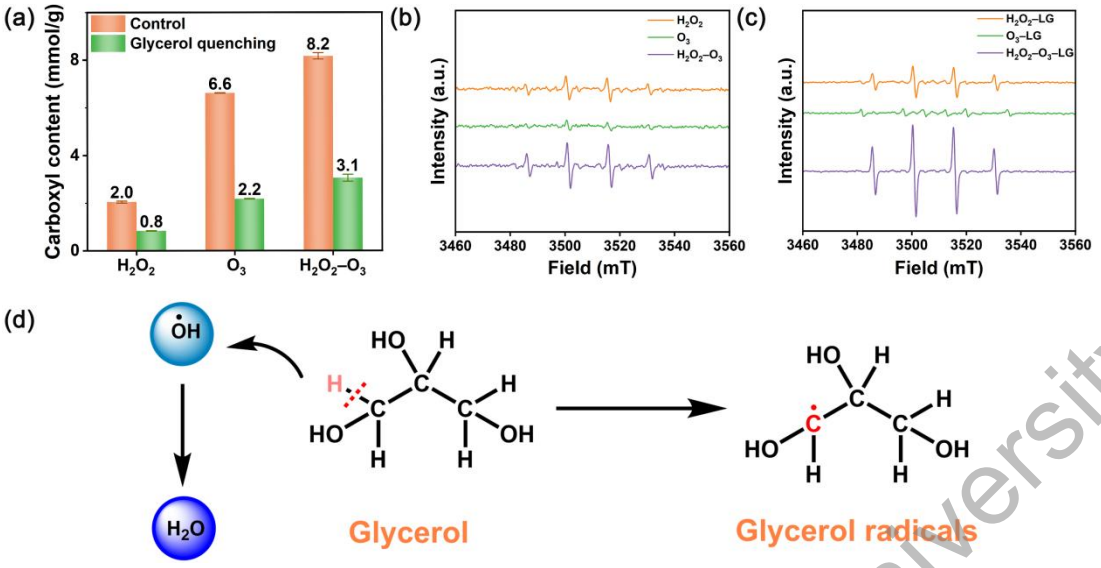

Fig. 6. Carboxyl content before and after glycerol quenching (a); EPR spectra of DMPO/·OH adducts in different oxidation systems: without lignin (b) and with lignin (c); Proposed mechanism of hydroxyl radical quenching by glycerol (d).

3.4. Oxidation mechanisms of different oxidation systems

Given the complex structure of lignin, precisely determining its oxidation reaction pathways poses a challenge. Therefore, model compound (2-methoxy-4-propylphenol) was utilized to explore the oxidation process. Intermediate products formed during the oxidation reaction are identified via ESI-MS (Fig. 7). The oxidation pathways of model compound under three oxidation systems are analyzed, and the proposed pathways are presented in Fig. 8. For the H_2O_2 system, relatively few products are formed. Based on detailed analysis, the oxidation pathway is proposed as follows (Fig. 8a): Initially, the side chain is oxidized to hydroxyl, aldehyde, or carboxyl groups by HO^+ or ·OH. Subsequently, it is transformed into conjugated substituted ortho– or para–quinone structures (e.g., 2–methoxy–1,4–benzoquinone) (Ma et al., 2014). Under the action of hydroxyl radicals, the benzene ring undergoes ring-opening to form conjugated aliphatic carboxylic acids (e.g., maleic acid), which are further oxidized to saturated aliphatic carboxylic acids (e.g., malonic acid). For the O_3 system, there are two main pathways (Fig. 8b): 1) Direct ozonation generates criegee intermediates, which induce ring-opening of the benzene ring to form unsaturated aliphatic carboxylic acids (e.g., 3–propyl–hex–3–en–2,5–dioic acid). These

unsaturated products further undergo criegee reactions to form aliphatic carboxylic acids (e.g., 2–propylsuccinic acid) (Kulwinder et al., 2022); 2) Electrophilic substitution reactions occur when ozone reacts with negatively charged atoms on the benzene ring, replacing hydrogen atoms to form intermediate products. After deoxygenation, these intermediates substitute Ph-OHs. Subsequently, under O_3 oxidation, the benzene ring undergoes ring-opening to form aliphatic carboxylic acids. Additionally, a small number of ·OH oxidation reactions occur during O_3 oxidation (Kulwinder et al., 2022). However, unlike H_2O_2, the products in this pathway primarily form aliphatic carboxylic acids or aldehydes via criegee reactions involving O_3 and unsaturated double bonds. As for the H_2O_2–O_3 oxidation system, since more ·OH radicals are generated during the reaction and O_3 acts as a highly reactive oxidant, multiple oxidation pathways exist for unsaturated bonds in this system (M'Arimi et al., 2020). The hydroxyl groups on the aliphatic side chains of the model compound are oxidized to carbonyl groups, leading to the formation of additional oxidation intermediates (e.g., oxalic acid and 2-carbonylsuccinic acid, as shown in Fig. 8c). Simultaneously, the presence of stronger oxidizing agents and faster reaction kinetics leads to the formation of smaller aliphatic carboxylic acids, including oxalic acid and glyoxylic acid. This indicates that lignin oxidation in the H_2O_2–O_3 system results in products with a lower *M*w and greater diversity. In conclusion, the analysis of intermediate products from model compound oxidation reveals that the H_2O_2–O_3 system exhibits excellent decolorization performance, high carboxyl content, and low *M*w. This is attributed to the generation of more ·OH radicals, the presence of multiple reaction pathways and diverse intermediate products.

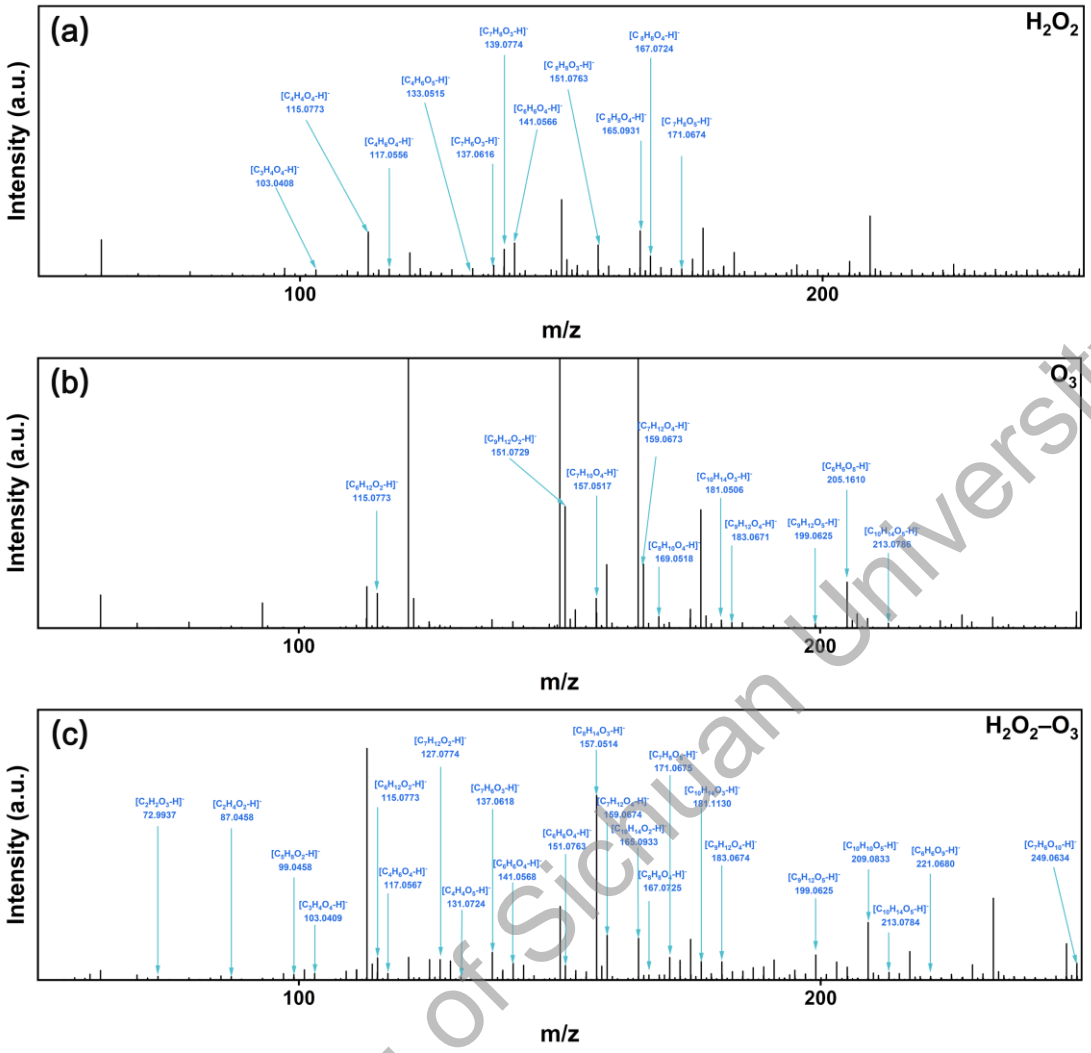

Fig. 7. ESI-MS spectra of lignin model compounds (2-Methoxy-4-propylphenol) oxidized by H_2O_2 (a); O_3 (b); H_2O_2–O_3 (c).

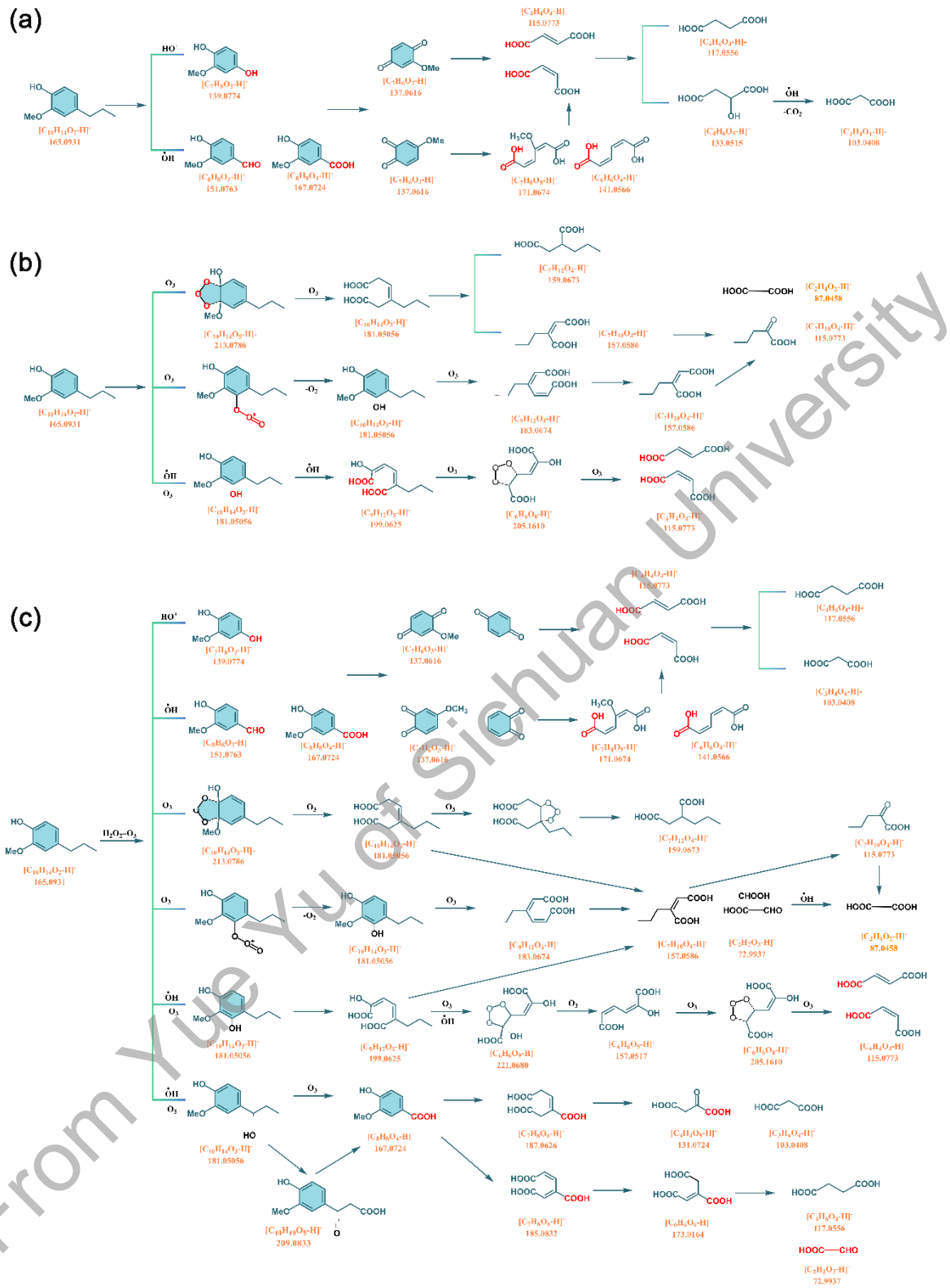

Fig. 8. Proposed oxidation pathways of the lignin model compound by H_2O_2 (a), O_3 (b), and H_2O_2–O_3 (c).

3.5. Retanning performance of OLGs

AS and OSLs with varying degrees of oxidation were utilized for the retanning of wet blue leather. OSL-retanned leathers demonstrated higher Ts (> 108.6°C) compared to the control (106.7°C) (Fig. 9a), suggesting that all OSLs exhibit a certain tanning effect and can improve the tanning performance of retanned leather. Additionally, OSL-retanned leathers showed a significantly higher thickness increase rate (22.7%–25.3%) relative to the control (8.6%) (Fig. 9b), as well as a comparable thickness increase rate (23.5%) to AS, thereby confirming the superior filling effect of OSLs as retanning agents. Notably, OSL2, with its appropriate functional groups and *M*w, exhibited excellent mechanical strength (Fig. 9c), softness (Fig. 9d), and fullness (Figs. 9e–f) compared to AS, demonstrating that OSL2 can serve as a viable alternative for retanning. Conversely, OSL1 and OSL3, which possess unsuitable chemical structures, displayed inferior retanning performance compared to AS. Therefore, reasonably controlling the structure of OSL is essential for developing an ideal lignin-based retanning agent. We further assessed the environmental benefits of AS and OSL during the retanning process (Fig. 10). The results indicated that OSL reduced carbon emissions by 61.7% and resource consumption by 71.6% compared to AS. Moreover, OSL exhibited low ecological and human toxicity, suggesting its fesible application potential as a retanning agent.

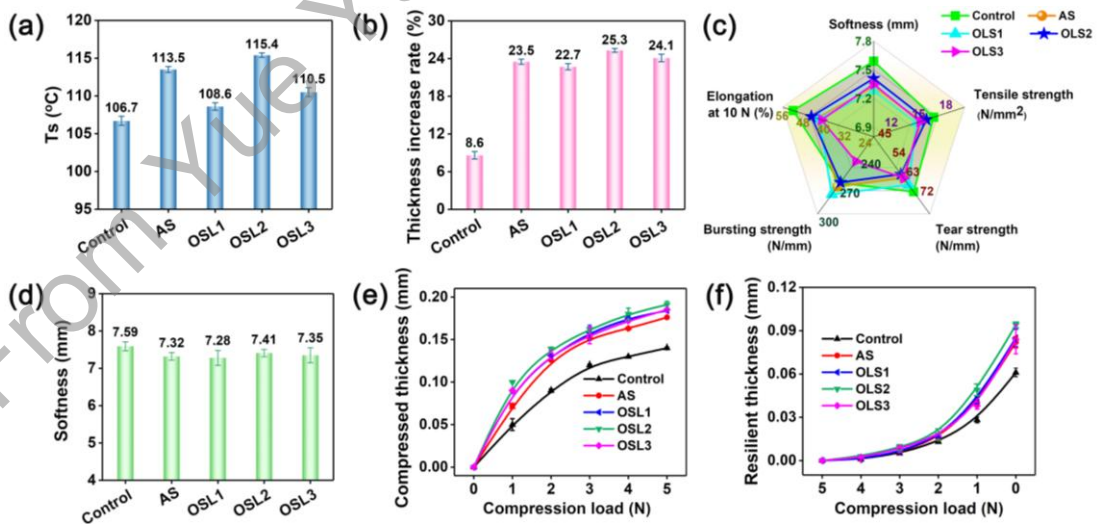

Fig. 9. Ts (a), thickness increase rate (b), physical and mechanical properties (c), softness (d), compression performance (e), and resilience performance (f) of crust leathers.

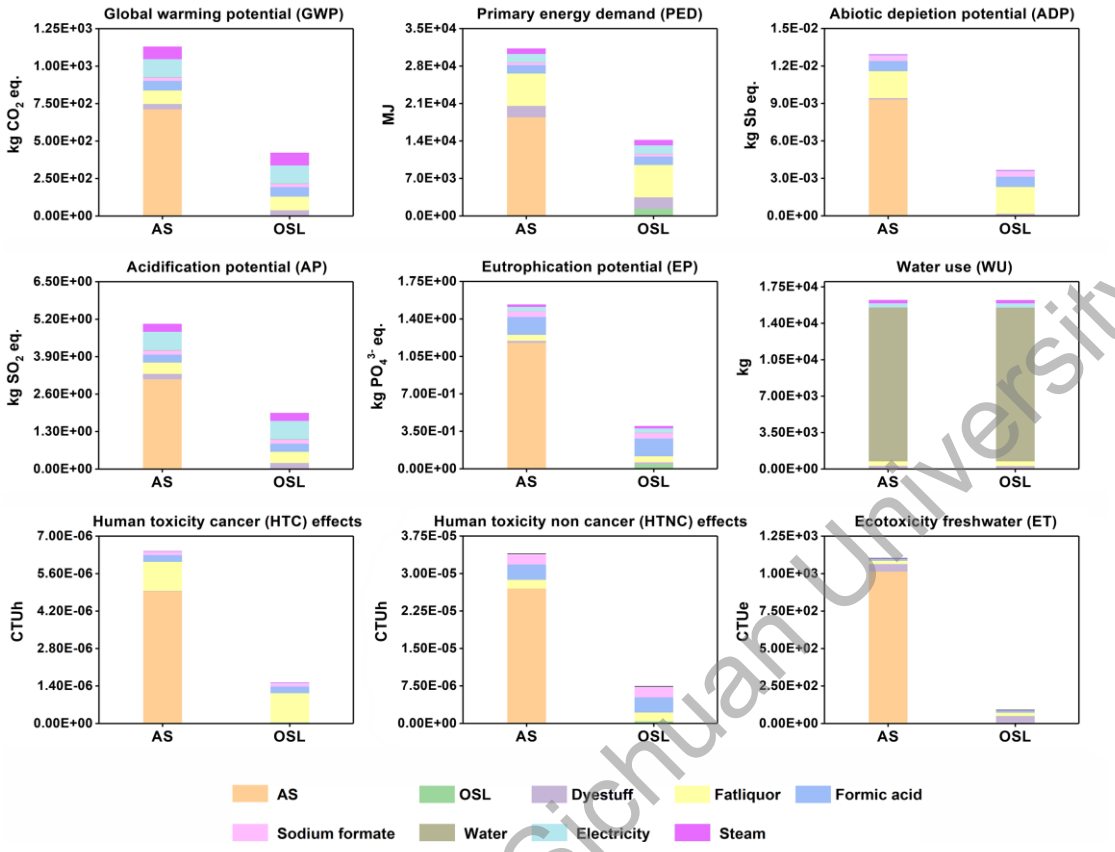

Fig. 10. Comparison of LCA results between AS and OSL retanning systems.

4. Conclusions

An H_2O_2–O_3 oxidation system with a synergistic decolorization effect for lignin (LG) was developed. The H_2O_2–O_3-treated LG exhibited optimal properties, including the lowest chromaticity (ΔE), highest carboxyl content (8.2 mmol/g), and reduced *M*w (735). Cleavage of β-O-4', β-5', and β-β' bonds contributed to the reduction in *M*w, while aromatic ring-opening reactions introduced carboxyl groups and disrupted conjugation. The H_2O_2–O_3 system generated twice as many ·OH radicals as H_2O_2 system alone, further enhanced by the presence of LG. O_3 primarily produced $\cdot O_2^-$ radicals via direct oxidation. While all three systems (H_2O_2–O_3, H_2O_2, and O_3) yielded aliphatic carboxylic acids, their reaction pathways differed: H_2O_2 relied on ·OH-mediated oxidation, O_3 formed Criegee intermediates, and H_2O_2–O_3 combined both pathways while generating a variety of active species and intermediates, enabling efficient small-acid generation. As a retanning agent, OSL2 formed robust Cr(III)-collagen networks via

carboxyl/phenolic hydroxyl coordination, achieving a shrinkage temperature (Ts) of 115.4°C with superior softness and mechanical properties. Compared with the conventional AS retanning system, OSL reduced carbon emissions by 61.7% and resource consumption by 71.6%. This work establishes a sustainable lignin-based retanning strategy, providing theoretical insights into lignin valorization and advancing eco-friendly leather manufacturing.

References

Balasubramanian P, Ramalingam S, Rao JR, et al., 2017. ***ACS Sustain Chem Eng***. 5, 7020-7029.

Espinoza-Acosta JL, Torres-Chavez PI, Olmedo-Martínez JL, et al., 2018. ***J Energy Chem***. 27, 1422-1438.

Jiang ZC, Ma Y, Guo XJ, et al., 2021. ***J Hazard Mater***. 403, 123701.

Liu GT, Yu Y, Zeng YH, et al., 2022. ***Leather Sci Eng.*** 32, 6-13. (In Chinese)

Ning GQ, Zhou JB, Liao XP, et al., 2022. ***J Am Leather Chem Assoc***. 117, 288-295.

Sen S, Patil S, Argyropoulos D S, 2015. ***Green Chem***. 17, 4862-4887.

Sun QY, Zeng YH, Wang YN, et al., 2021. ***J Leather Sci Eng.*** 3, 31.

Thanikaivelan P, Mohan CR, Saravanabhavan S, et al., 2007. ***J Am Leather Chem Assoc***. 102, 306-314.

Vedhanayagam M, Teddy TK, Sreeram KJ, et al., 2015. ***J Am Leather Chem Assoc***. 110, 295-301.

Yadav M, Gole VL, Sharma J, et al., 2022. ***J Environ Health Sci.*** 20, 889-898.

Zakir, MJA, Ramalingam S, Balasubramanian P, et al., 2015. ***J Clean Prod***. 104, 436-444.

Fika Andriani, Martin Lawoko, 2024. ***Biomacromolecules.***25,4246-4254.

Figueiredo, M.B., Heeres, H.J., et al., 2020. ***Sustainable Energy Fuels.*** 4, 265–276.

J. Wang, H. Chen, 2020. ***Sci. Total Environ.*** 704, 135249.

Nozomi Takeuchi, Hideaki Mizoguchi, 2017. ***Chem Eng J.*** 313, 309-316.

Fei Chen, Yi-Shuo Zhang, et al., 2024. ***Chem Eng J.*** 483, 149129.

Yu, Y., Wang, Y.N., et al., 2017. ***Polym***. 174, 823–829.

Wang, J.Y., Yu, Y., et al., 2022a. ***Carbohydrate Research***. 511, 108501.

Zhang, S.M., Zheng, C., et al., 2022b. ***Compos. Part B-Eng***. 234, 109669.

Belasco, R., Edwards, T., et al., 2020. ***Front. Nutr***. 7, 576974.

Hwang S C, Huling S G, et al., 2010. ***Chemosphere***. 78, 563-568.

Qingguo Zhou, Zhongyang Luo, et al.,2020. ***J Anal Appl Pyrol.*** 152, 104948.

Yu, Y., Zeng, Y.H., et al., 2020. ***J. Am. Leather Chem.*** 115, 176–182.

Guo, X.R., Yu, Y., et al., 2021. ***J. Am. Leather Chem***. 116, 155–161.

Covington, et al., 1997. ***Chem. Soc. Rev.*** 26, 111–126.

Shen, H.C., Cui, C.F., et al., 2022. ***Sep. Purif. Technol.*** 281, 119885.

André Fernandesa, Michał Gągola, et al., 2019. ***Sep. Purif. Technol.*** 224, 1-14.

Dong, C.Y., Meng, X.Z., et al., 2022. ***Ind. Crop. Prod.*** 185, 115130.

Jiang, Z.C., Ma, Y., et al., 2021. ***J. Hazard. Mater.*** 403, 123701.

Areskogh, D., Li, J., et al., 2010. ***Ind. Crop. Prod.*** 32, 458–466.

Kulwinder Kaur, R. Pandiselvam , et al., 2022. ***Food Control***. 142, 109207.

Boqiang Li, Baiyang Chen et al., 2024. ***J. Hazard. Mater.*** 478,135502.

Ruoshui Ma, Mond Guo, et al., 2014. ***ChemSusChem***. 7, 412-415.

Dongdong Ge, Shouqiang Huang, et al., 2022. ***J Clean Prod.*** 359, 132049.

Wu, Q.Y., Yang, Z.W., et al., 2021. ***J. Hazard Mater.*** 418, 126327.

M.M. M'Arimi, C.A. Mecha, et al., 2020. ***Renewable and Sustainable Energy Reviews.*** 121, 109669.

Arulselvan Ponnudurai, Peter Schulze, et al., 2023. ***ACS Sustain Chem Eng.*** 11, 766-776.

Xue, P.B., Yu, Y., et al., 2024. ***Ind. Crop. Prod.*** 208, 117916.

Hilde V. Halleraker, Solmaz Ghoreishi, et al., 2020. ***Results in Chemistry.*** 2, 100019.

Kulwinder Kaur, R. Pandiselvam., 2022. ***Food Control.*** 142, 109207.

Ma, C.H., Zhang, J.F., et al., 2024. ***Trends in Chemistry.*** 6, 234-247.

Md. Sohel Rana, Marcelo I. Guzman, 2020. ***J. Phys. Chem. A.*** 124, 8822-8833.

Tan, S.W., Long, K., et al., 2024. ***J. Environ. Manage.*** 358, 120896.

Zhou, A.Y., Shen, Y., et al., 2025. ***J. Anal. Appl. Pyrol.*** 106966.

Han, Y., Wei, B.J., et al., 2023. ***J. Mol. Liq.*** 369, 120966.

Xie, J.X., Zheng, Y., et al., 2023. ***Applied Catalysis B: Environmental.*** 320, 121935.

Zhang, L., Fu, J.J., et al., 2025. ***Int. J. Biol. Macromol.*** 292, 139131.

Ruoshui Ma, Mond Guo, et al., 2014. ***ChemSusChem.*** 7, 412-415.

Du, X.J., Wu, S.B., et al., 2022. ***Int. J. Biol. Macromol.*** 231, 107232.